Accepted Manuscript

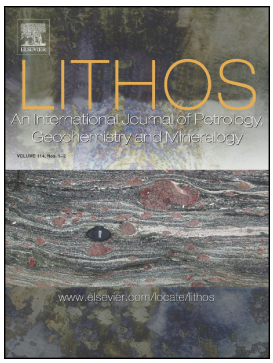

The evolution and ascent paths of mantle xenolith-bearing magma: Observations and insights from Cenozoic basalts in Southeast China

Pu Sun, Yaoling Niu, Pengyuan Guo, Huixia Cui, Lei Ye, Jinju Liu

PII: S0024-4937(18)30142-7
DOI: doi:10.1016/j.lithos.2018.04.015
Reference: LITHOS 4631

To appear in:

Received date: 20 November 2017
Accepted date: 17 April 2018

Please cite this article as: Pu Sun, Yaoling Niu, Pengyuan Guo, Huixia Cui, Lei Ye, Jinju Liu , The evolution and ascent paths of mantle xenolith-bearing magma: Observations and insights from Cenozoic basalts in Southeast China. The address for the corresponding author was captured as affiliation for all authors. Please check if appropriate. Lithos(2018), doi:10.1016/j.lithos.2018.04.015

The evolution and ascent paths of mantle xenolith-bearing magma: Observations and insights from Cenozoic basalts in Southeast China

Pu Sun [1, 2, 3 *], Yaoling Niu [1, 2, 4, 5 **], Pengyuan Guo [1, 2], Huixia Cui [6], Lei Ye [6], Jinju Liu [6]

[1] Institute of Oceanology, Chinese Academy of Sciences, Qingdao 266071, China

[2] Laboratory for Marine Geology, Qingdao National Laboratory for Marine Science and Technology, Qingdao 266061, China

[3] University of Chinese Academy of Sciences, Beijing 100049, China

[4] Department of Earth Sciences, Durham University, Durham DH1 3LE, UK

[5] School of Earth Science and Resources, China University of Geosciences, Beijing 100083, China

[6] School of Earth Sciences, Lanzhou University, Lanzhou 730000, China

Correspondence:

* Mr. Pu Sun (pu.sun@foxmail.com)

** Professor Yaoling Niu (yaoling.niu@durham.ac.uk)

Abstract. Studies have shown that mantle xenolith-bearing magmas must ascend rapidly to carry mantle xenoliths to the surface. It has thus been inferred inadvertently that such rapid ascending melt must have undergone little crystallization or evolution. However, this inference is apparently inconsistent with the widespread observation that xenolith-bearing alkali basalts are variably evolved with $Mg^{\#} \leq 72$. In this paper, we discuss this important, yet overlooked, petrological problem and offer new perspectives with evidence.

We analyzed the Cenozoic mantle xenolith-bearing alkali basalts from several locations in Southeast China that have experienced varying degrees of fractional crystallization ($Mg^{\#}$ = ~ 48-67). The variably evolved composition of host alkali basalts is not in contradiction with rapid ascent, but rather reflects inevitability of crystallization during ascent. Thermometry calculations for clinopyroxene (Cpx) megacrysts give equilibrium temperatures of 1238-1390 ℃, which is consistent with the effect of conductive cooling and melt crystallization during ascent because $T_{Melt} > T_{Lithosphere}$. The equilibrium pressure (18-27 kbar) of these Cpx megacrysts suggests that the crystallization takes place under lithospheric mantle conditions. The host melt must have experienced limited low-pressure residence in the shallower levels of lithospheric mantle and crust. This is in fact consistent with the rapid ascent of the host melt to bring mantle xenoliths to the surface.

Key words: alkali basalts, magma evolution, mantle xenoliths, magma chamber, clinopyroxene megacryst, thermobarometry

1. Introduction

Our present-day knowledge on the thermal structure of sub-continental lithospheric mantle (SCLM) largely comes from petrological, geochemical, experimental and thermodynamic studies of mantle xenoliths brought to the surface by kimberlite eruptions, and most abundantly by eruptions of alkali basalts (e.g., O'Hara and Schairer, 1963; O'Hara, 1967; Wood and Banno, 1973; Menzies, 1983; Nickel and Brey, 1984; Herzberg, 1993; Rudnick et al., 1998; Sleep, 2005; Mather et al., 2011). The worldwide observation that apart from kimberlite, it is alkali basalt (vs. tholeiite) that carries mantle xenoliths to the surface, points to a genetic link between mantle xenoliths and alkali basaltic magmatism. Because mantle xenoliths are lithospheric mantle materials whereas basaltic melts are derived from the asthenosphere at greater depths, it follows that alkali basaltic melts that are enriched in volatiles and alkalis have the capacity to collect and transport lithospheric mantle materials during ascent.

Indeed, reduced solubility of volatiles in the melts with decreasing pressure will result in volatile exsolution during alkali melt ascent, causing the bulk magma volume expansion and viscosity increase with destructive power to break magma conduits in the lithospheric mantle (Spera, 1984; Woods and Cardoso, 1997; Lensky et al., 2006; Gonnermann and Manga, 2013). These broken fragments of lithospheric material are the familiar "mantle xenoliths" carried in alkali basalts during eruption. However, mantle xenoliths are physically denser than, and compositionally not in equilibrium with the host melt, which requires the host melts ascend rapidly, with the aid of increased viscosity due to volatile exsolution and bubble formation, to transport

mantle xenoliths to the surface. The ascending rates of mantle xenolith-bearing alkali magmas have been estimated to be 6 ± 3 m/s and 0.2-2 m/s by Demouchy et al. (2006) and O'Reilly and Griffin (2010), respectively, which is consistent with the anticipation of the rapid ascent of xenolith-bearing melt.

The "primary" basaltic melt after being extracted from the asthenospheric source region will undergo varying extent of crystallization during ascent, mostly as a consequence of magma cooling (Niu, 1997, 2005; O'Hara and Herzberg, 2002; Niu and O'Hara, 2008). One may anticipate that the rapid ascending xenolith-bearing melt would undergo little crystallization (Wass, 1980; Higgins et al., 1985; O'Reilly and Griffin, 1984; Sigmarsson et al., 1998; McBride et al., 2001). However, this inference is inconsistent with the widespread observation that the xenolith-bearing alkali basalts are variably evolved with $Mg^{\#} \leq 72$, which is the minimum value required for the melt to be in equilibrium with mantle olivine in both asthenospheric source region and lithospheric mantle magma conduit. Irving and Price (1981) interpreted some evolved lherzolite-bearing phonolitic lavas from Nigeria, Australia, East Germany and New Zealand as originating from fractional crystallization of basanitic magmas in the upper mantle, which is reasonable and likely. However, this apparent problem still remains rarely addressed until recently when pyroxenites were popularly invoked as source for ocean island basalts (OIB) and alkali basalts (Sobolev et al., 2005, 2007; Yang and Zhou, 2013) with the conclusion that the more evolved host magmas must have derived from pyroxenites, which has many more problems than certainties (see Niu and O'Hara, 2003, 2007; Niu et al., 2011, 2012; Niu, 2016).

We consider that the variably evolved nature of host melts does not negate the rapid ascent of mantle xenolith-bearing melt but emphasizes the importance of melt crystallization during ascent. In this paper, we use bulk-rock major and trace elements and clinopyroxene thermobarometry of several sample suites from Southeast (SE) China as a case study to address the above fundamental yet overlooked petrological problems of global significance. We conclude that the varying extent of crystallization during rapid ascent is inevitable for mantle xenolith-bearing basaltic melts, which in SE China largely take place in magma chambers in lithospheric mantle.

2. Geological background and analytical procedures

2.1 Geological background

Cenozoic basaltic volcanism is widespread in eastern China (Fig. 1a). These basalts have been identified as typical continental-intraplate basalts derived from the asthenosphere, with trace element signatures similar to ocean island basalts (OIB) (Tu et al., 1991; Zou et al., 2000; Wang et al., 2011; Meng et al., 2015). A significant low-degree melt metasomatism within the asthenospheric mantle has been invoked to explain the incompatible element enrichment in these basalts (Niu, 2005, 2014; Guo et al., 2016; Sun et al., 2017).

In SE China, the Cenozoic basaltic volcanism is spatially associated with three extensional fault systems parallel to the coastline (Fig. 1b; Chung et al., 1994; Ho et al., 2003; Huang et al., 2013; Sun et al., 2017). Basalts containing abundant mantle

xenoliths were collected from several localities (i.e., Xiadai, Xiahuqiao, Dayangke and Jiucaidi) (see Fig. 1b and Appendix A for sample locations). The mantle xenoliths are 4-10 cm in size (Figs. 2a & b) and are dominated by spinel lherzolite and harzburgite with minor dunite. Clinopyroxene (Cpx) megacrysts with varying size of ~ 1-6 cm are common in these samples except for those from Xiahuqiao (Figs. 2c & d). They are optically homogeneous with 0.5-1.0 mm gray or brown reaction rims (Figs. 2e & f). In addition to xenoliths, these basalts contain abundant euhedral to subhedral olivine (Ol) and relatively less Cpx phenocrysts in a fine-grained and microlite-bearing groundmass (Figs. 2g & h). The Ar-Ar dating gives eruption ages of 20.2 ± 0.1Ma for basalts from Jiucaidi, 23.3 ± 0.3 Ma from Xiadai, 9.4 ± 0.1 Ma from Xiahuqiao, 2.2 ± 0.1 Ma from Dangyangke (Ho et al., 2003; Huang et al., 2013).

2.2 Analytical procedures

As we endeavored to study melt compositions by choosing glasses if any, or quenched matrix materials, we crushed fresh samples to chips of ≤ 5 mm to exclude phenocrysts, xenocrysts and weathered surfaces before repeatedly washing the chips in Milli-Q water, drying them and then ground them into powders with an agate mill. Despite the effort, our analyses still contain contributions from olivine micro-phenocrysts (Figs. 2g & h), rather than melt compositions we endeavored to obtain. In our case, we made corrections for this problem using the method described in Sun et al. (2017) and also a new method to verify the validity of the correction results (see Appendix B).

Major and trace element analysis of glasses/matrix powders was done at China University of Geosciences in Beijing (CUGB). The major element analysis was done using a Leeman Prodigy Inductively Coupled Plasma Optical Emission Spectrometer (ICP-OES) and trace element analysis was done using an Agilent 7500a Inductively Coupled Plasma Mass Spectrometer (ICP-MS). Repeated analyses of USGS reference rock standards AGV-2, W-2, BHVO-2 and national geological standard reference materials GSR-1, GSR-3 give analytical precision better than 15% for Ni, Co, Cr and Sc and better than 5% for other trace elements. The analytical details are given in Song et al. (2010).

Major elements and Cr contents of Cpx megacrysts were analyzed in thin sections using LA-ICP-MS in Institute of Oceanology, Chinese Academy of Sciences. Laser sampling was performed using a Photon Machines Excite 193 nm excimer Ar–F laser system, and an Agilent 7900a ICP-MS instrument was used to acquire ion-signal intensities. The samples were analyzed using a 40 μm spot and 7.42 J/cm^2 energy density at a repetition rate of 6 Hz. Each analysis includes 25s background acquisition (gas blank) followed by 50s data acquisition. USGS glasses (BCR-2G, BHVO-2G and BIR-1G) are used as external standards for calibration. Every five sample analyses were followed by two analyses of GSE-1G (one as QC to correct for the time-dependent drift of sensitivity and the other as an unknown sample to check for analytical accuracy and precision). The raw data were processed using ICPMSDataCal (Liu et al., 2008). Repeated analysis of GSE-1G give analytical precision and accuracy generally better than 5% for major elements and Cr except for P_2O_5. The analytical data include 231 spot analyses from 26 single Cpx megacrysts, with 5 to 16 points in a profile per Cpx crystal. The analytical details are given in Xiao et al. (2018, in preparation).

3. Data and interpretations

3.1 The geochemistry of mantle xenolith-bearing basalts

The analytical data are given in Appendix A. After correction for the olivine phenocryst effects (see Appendix B for correction results), these basalts have variably high alkali contents with total alkalis ($Na_2O + K_2O$) of 2.47 – 8.03 wt. %, and range from tephrite/basanite, trachybasalt to alkali basalt in the TAS diagram (Fig. 3). They show a wide MgO range (5-12 wt.%) with varying $Mg^{\#}$ (= $100\times Mg/[Fe^{2+}+Mg]$) of 48-67, indicating variable extent of evolution from the expected primary magma (i.e., $Mg^{\#} \geq 72$) in equilibrium with mantle olivine. Although scattered, there exist first order systematic variations as a function of $Mg^{\#}$ (Fig. 4) using samples from Jiucaidi (also see below). These correlated variations of major elements, trace elements and their ratios are to a first order consistent with varying extents of fractional crystallization dominated by olivine and Cpx.

As shown in Fig. 5a, mantle xenolith-bearing alkali basalts have rare earth element (REE) patterns similar to that of the present-day OIB, but most of them are more enriched in light REEs with high $[La/Sm]_N$ (2.68 – 4.33), $[La/Yb]_N$ (14.4 – 40.4) and $[Dy/Yb]_N$ (2 – 3) ratios. In Fig. 5b, they have multi-element patterns similar to that of OIB but are more enriched in the progressively more incompatible elements with significantly greater $[Nb/Th]_N$, $[Ta/U]_N$ and $[P/Sm]_N$ than unity (i.e., positive Nb,

Ta and P anomalies common to oceanic basalts; Niu and Batiza, 1997). Even though fractional crystallization can result in the enrichment of progressively more incompatible elements (i.e., increasing La, Sm, La/Sm and Sm/Yb with decreasing $Mg^{\#}$; Fig. 4), this process is apparently inadequate to explain the overall extremely enriched incompatible elements and depleted heavy REEs in these basalts (Fig. 5). Therefore, the characteristics of these mantle xenolith-bearing basalts are most consistent with an origin of low extent of partial melting from an enriched mantle source with garnet present as a residual phase as indicated by heavy REE depletion with high $[Dy/Yb]_N > 1$ (Sun et al., 2017).

3.2 Geochemistry of clinopyroxene (Cpx) megacrysts

The compositions of Cpx megacrysts are given in Appendix C. They have relatively low SiO_2 (47.3-53.6 wt. %), Cr_2O_3 (0.00-0.62 wt. %), $Mg^{\#}$ (64.5-85.2) and TiO_2 (0.38-1.69 wt. %) but high Al_2O_3 (6.34-9.22 wt. %), which is different from mantle-derived Cr-diopside (high SiO_2, Cr_2O_3 and $Mg^{\#}$), but similar to Al-augite crystallized at high pressures (Wass, 1979; Irving and Frey, 1984). Overall, variations in Cpx components are limited to the range of Wo_{35-47}, En_{35-53}, Fs_{9-19}, which are classified as diopside and augite (Fig. 6a). In addition, the composition for a single Cpx megacryst is generally homogeneous (Fig. 6b). In the following, multiple analyses in an individual Cpx megacryst are averaged to obtain the mean composition of the Cpx crystal.

These Cpx megacrysts show significant correlations of $Mg^{\#}$ with major elements (e.g., SiO_2, TiO_2, Al_2O_3, FeO and Na_2O) and Cr (Fig. 7), showing their derivation

from melts that had experienced variable extent of fractional crystallization. Three Cpx megacrysts (XD11-11A, XD11-11C and JC11-03A) have apparently lower $Mg^{\#}$ (65-69), SiO_2 and Cr, and higher TiO_2, Al_2O_3, FeO and Na_2O, compared with other Cpx megacrysts ($Mg^{\#}$ = 75-84), reflecting their crystallization from compositionally more evolved melts.

4. Discussion

4.1 Fractional crystallization reflected from basalt compositions

Mantle xenolith-bearing basaltic magma has been inferred to ascend rapidly (Demouchy et al., 2006; O'Reilly and Griffin, 2010), which would suggest less heat loss, less temperature drop and less crystallization during ascent. This reasoning is logical. However, the mantle xenolith-bearing basalts in SE China have $Mg^{\#}$ of 48-67, which manifests in simple clarity that they must have experienced significant crystallization from their primary state ($Mg^{\#} \geq 72$) in equilibrium with mantle olivine. Because mantle melting processes exert the primary control on the compositions of basalts from different locations in SE China (Sun et al., 2017), we select basalts from a single location of Jiucaidi where sufficient samples with a large compositional spectrum exists to evaluate the effect of fractional crystallization during magma ascent.

In Fig. 4, these samples show negative correlations between $Mg^{\#}$ and incompatible major and trace elements (K_2O+Na_2O, TiO_2, P_2O_5, La and Sm), and

positive correlations between $Mg^{\#}$ and Cr and Ni. All these elemental systematics are consistent with olivine and Cpx being the dominant liquidus phases during cooling and fractional crystallization, most likely at high pressures without plagioclase on the liquidus as manifested by decreasing CaO/Al_2O_3 ($\boldsymbol{Kd}_{cpx}^{\frac{CaO}{Al2O3}} >> \boldsymbol{Kd}_{plagioclase}^{\frac{CaO}{Al2O3}}$) and increasing La/Sm and Sm/Yb with decreasing $Mg^{\#}$ ($\boldsymbol{Kd}_{Yb}^{cpx/melt} > \boldsymbol{Kd}_{Sm}^{cpx/melt} > \boldsymbol{Kd}_{La}^{cpx/melt}$; e.g. Blundy et al., 1998); Sm/Yb is essentially constant in the course of low-pressure fractional crystallization dominated by olivine + plagioclase with Cpx appearing late (MgO < ~ 8 wt.%) on the liquidus (Niu and O'Hara, 2009), but in the basalts under consideration here, Sm/Yb increases with decreasing $Mg^{\#}$. This is consistent with our petrological observation of abundant olivine phenocrysts and Cpx phenocrysts and megacrysts entrained in these basalts.

4.2 Is variably high extent of crystallization possible during ascent of xenolith-bearing magma?

4.2.1 Cpx thermobarometer

There are generally two kinds of thermobarometers to calculate the equilibrium temperature and pressure of Cpx phenocryst and megacryst crystallization. The most widely used thermobarometer is based on the jadeite-diopside/hedenbergite exchange equilibria between Cpx and host melt (Cpx-melt thermobarometer; Putirka et al., 1996; Putirka et al., 2003), which is most precise with least systematic error. The other

thermobarometer is based only on the Cpx components (single Cpx thermobarometer; Nimis, 1995, 1999; Nimis and Taylor, 2000), which is also valid but contains systematic errors (Putirka, 2008).

The Cpx-melt thermobarometer needs approximation of the melt compositions in equilibrium with the Cpx. Bulk-rock compositions have been most commonly approximated as representing the melt. However, the bulk-rock could represent melt only when the bulk-rock acted as a closed system (Putirka, 2008). The presence of mantle peridotite xenoliths in these rocks clearly negates the bulk-rock as a closed system. As stated above, bulk-rock compositions rarely represent pure melt, but mixture of crystals (e.g. olivine and Cpx) and melts. Therefore, using bulk-rock compositions in Cpx thermobarometer calculation may give misleading results.

Using Cpx from Jiucaidi as an example, we illustrate the above problem in Fig. 8 by using the Cpx-melt thermobarometer in Putirka et al. (2003). The standard error of estimate (SEE) for this method is ± 33 ºC and ± 1.7 kbar. Nominal melts needed by this thermobarometer are approximated by the uncorrected bulk-rock compositions (samples with $Mg^{\#}$ of 56, 60 and 65; Fig. 8a) and bulk-rock compositions corrected for the olivine effect (samples with $Mg^{\#}$ of 48, 53 and 59; Fig. 8b), respectively. Although our corrected "melts" may not be perfect due to minute olivine and minor Cpx effect, they are adequately close to melt compositions. We consider that Cpx crystals plotted within the $K_D[Fe\text{-}Mg]^{Cpx\text{-}melt}$ = 0.28±0.08 interval are in equilibrium with the nominal melts (Putirka, 2008; Fig. 8a & b). Figure 8c shows the results calculated using uncorrected bulk-rock compositions as "melts", which gives

crystallization temperatures and pressures of 1250-1304 ºC and 16-21 kbar, respectively. Figure 8d shows the results calculated using the corrected "melt", which gives lower crystallization temperatures and pressures of 1213-1270 ºC and 12-16 kbar, respectively. These calculation results indicate that (1) the calculated temperature and pressure values using the Cpx-melt thermobarometer highly depend on the nominal melt compositions chosen (Fig. 8c & d); (2) compared with the thermobarometry calculations using corrected "melt" compositions, calculations using uncorrected bulk-rock compositions give over-estimated temperature and pressure results (Fig. 8c & d). Therefore, using uncorrected bulk-rock compositions in the Cpx thermobarometer calculation may give misleading results; (3) although the Cpx-melt thermobarometer is considered as most precise with least systematic error, choosing different nominal melts can introduce significant errors in this thermobarometer. For example, in Fig. 8d, except for the systematic errors of ± 33 ºC and ± 1.7 kbar, uncertainties in the nominal melt compositions would lead to additional 57 ºC and 4 kbar derivations in the calculated temperature and pressure values, which is geologically rather significant. Therefore, caution is needed when using the Cpx-melt thermobarometer to obtain precise temperature and pressure values.

Considering the potential errors of the Cpx-melt thermobarometer, we choose to use the single Cpx thermobarometer to calculate the crystallization temperatures and pressures of these Cpx megacrysts. The Cpx barometer and thermometer we use are recalibrated from Nimis (1995) and Nimis and Taylor (2000), respectively (Putirka, 2008; equation 32a/32d), which are more precise than their original forms, but still

contain systematic errors (~ ± 3.1 kbar and ± 58 ℃). The calculated *P-T* results are listed in Appendix D and shown in Figure 9. These Cpx megacrysts from SE China crystallized under conditions of 18-27 kbar and 1238-1390 ℃. Given the uncertainties in these thermobarometers, we do not intend to rely on *P* and *T* values, but to emphasize the similarities and differences between Cpx samples and sample suites for comparison.

4.2.2 Cooling-induced crystallization during ascent

Figure 9 shows our calculated *P-T* conditions using the Cpx-thermobarometry (see above). For comparison, the lithosphere geotherm of eastern China (Menzies et al., 2007) and the solidus and liquidus of alkali olivine basalt (Green and Ringwood, 1967) are also plotted. Three Cpx megacrysts with lower $Mg^{\#}$ (XD11-11A, XD11-11C and JC11-03A; Fig. 7) have lower calculated crystallization temperatures more close to the lithosphere geotherm than other Cpx megacrysts (Fig. 9), which is consistent with our explanation of their crystallization from more evolved melts (Niu et al., 2002). According to the Fe-Mg exchange equilibrium ($Kd_{[Fe\text{-}Mg]}^{Cpx\text{-}Melt}$ = 0.28 ± 0.08; Putirka, 2008), the melts in equilibrium with these three Cpx megacrysts have low $Mg^{\#}$ of 34 – 38, compared with $Mg^{\#}$ = 48 – 67 of our basalt samples. We infer these three Cpx megacrysts crystallized from highly evolved melts that experienced long-time thermal equilibrium with ambient lithosphere wall-rock. Therefore, the calculated *P-T* results of these three Cpx megacrysts do not represent the *P-T*

conditions of rapidly ascending mantle-xenolith bearing melt.

In comparison, most of Cpx megacrysts show much higher temperatures than the ambient lithosphere, which is consistent with their parental melts crystallization during ascent because of the inevitable conductive heat loss to the cooler ambient mantle. Hence, the observed variably highly evolved composition of xenolith-bearing alkali basalts is not in contradiction with the rapid ascent, but an unavoidable consequence of melt crystallization because of cooling (heat loss to the ambient mantle).

4.2.3 Where does the crystallization take place?

To convert pressure (kbar) to depth (km), we estimated the approximate densities of the representative crustal and mantle layers beneath SE China (Appendix E; Zheng et al., 2001; Zhang and Wang, 2007) and created an equation relating depth to calculated pressure:

$$D\ (km) = 3.04*P\ (kbar) + 5.35 \quad [1]$$

The calculated pressures (18-27 kbar) translate into Cpx crystallization depth of 59-88 km (Appendix D). According to Li et al. (2006), the crustal thickness of South China is about 30-34 km and is 30-32 km in the coastal region, which means that all Cpx megacrysts must have crystallized at lithospheric mantle depths. This is consistent with previous thermobarometric calculations on Cpx megacrysts in eastern China (Huang et al., 2007; Chen et al., 2009).

During melt ascent with cooling, melt crystallization can take place both in the conduit and in a magma chamber. In Irving's "flow crystallization" model, crystallization takes place along the walls of magma conduits from a flowing melt (Irving, 1978, 1980). This is possible and likely, but the rapid melt ascent in magma conduits with continued decompression (1) does not guarantee sufficient time for crystal-melt equilibrium to form large compositionally uniform megacrysts (Fig. 6b); (2) crystallization on the conduit wall surface could further prevent the conduit wall destruction, xenolith generation and transport. Thus, under the conditions of rapid ascent, a magma conduit may not be the ideal place for crystallization. Furthermore, Irving's "flow crystallization" model discussed composite xenoliths in which the pyroxenites are composed of coarse but not megacryst-sized veins. Hence, magma conduit is not a likely site for megacryst growth. It follows indeed that magma chambers in a stable environment are required to allow slow cooling and the growth of compositionally uniform large crystals, that is, megacrysts (O'Hara, 1977; O'Hara and Mathews, 1981; Sparks et al., 1984). The abundant Cenozoic volcanism in eastern China and frequent melt supply from the source regions could ensure the existence of long-lived magma chambers in the lithospheric mantle (Niu and O'Hara, 2008). All this leads us to the proposal that xenolith-bearing alkali basalts in SE China must have evolved in magma chambers developed in the lithospheric mantle depths.

4.3 Ascent of mantle xenolith-bearing magmas beneath SE China

The calculated *T-P* results of the Cpx megacrysts suggest that their parental magmas must have crystallized under high pressures in lithospheric mantle and did

not experience long-time stay at crustal levels. This conclusion can also be inferred from the homogenous compositional profile of these Cpx megacrysts (Fig. 6b) and the absence of low-pressure overgrowth-induced compositional zonation (Dobosi, 1989; Neumann et al., 1999; Nakagawa et al., 2002; Stock et al., 2012; Geiger et al., 2016). In addition, the petrological observation of widespread mantle xenoliths entrained in these basalts indicates that the host melts may have ascended too rapidly to experience any residence in the shallow levels (> 20 m/s through shallow crust and > 300 m/s in the uppermost crust; O'Reilly and Griffin, 2010).

Based on the above observations and inferences, we provide a model for the ascent of mantle xenolith-bearing magmas beneath SE China (Fig. 10). That is, 1) low extent of partial melting of a fertile mantle source enriched in incompatible elements and volatiles produced alkali basaltic melts with elevated abundances of volatiles (Sun et al., 2017); 2) these melts migrated upwards from the source region, percolated through the base of the lithospheric mantle and focused in a magma chamber in the lithospheric mantle where variable extent of mineral crystallization (including Cpx megacryst) happened, (3) periodically melt replenishment in the magma chamber forced the residual melt together with the crystallized Cpx megacrysts to ascend from the magma chamber. Such alkali basaltic melts during ascent through the mantle lithosphere will exsolve volatiles (reduced volatile solubility in the melt due to decompression), resulting in bulk magma volume expansion, viscosity increase, and development of power to fragment the conduit wall-rock to produce "mantle xenoliths", and rapidly transport them to the surface with limited residence in shallow

levels. In addition, volatile exsolution during magma ascent and decompression can also increase liquidus temperatures, which may further facilitate melt crystallizations (Cashman and Blundy, 2000; Sparks et al., 2000; Blundy and Cashman, 2001, 2005).

5. Conclusions

1. After correction for the effect of olivine micro-phenocrysts in the samples, we obtained the compositions of melt with $Mg^{\#}$ = 48-67 for the Cenozoic xenolith-bearing alkali basalts from Southeast China. These highly evolved compositions are consistent with olivine-Cpx crystallization during ascent.
2. Calculations for equilibrium temperatures (1238-1390 ℃) of Cpx megacrysts show that their parental melt are hotter than the ambient lithosphere, which is consistent with cooling-induced crystallization during ascent.
3. The equilibrium pressures (18-27 kbar) of Cpx megacrysts suggest that the crystallization takes place under lithospheric mantle conditions. This could occur in magma conduits, but lithospheric mantle magma chambers are required to provide a stable environment for crystallizing megacrysts (1-6 cm) of uniform composition.
4. Melts entraining megacrysts after extracted from the magma chamber should experience limited residence in the shallow levels to rapidly transport mantle xenoliths to the surface.

Acknowledgements

We thank Maochao Zhang, Yanan Cong, Peiqing Hu and Junping Gao for field company and sample preparation. We also thank Li Su, Yuanyuan Xiao and Meng Duan for their analytical assistance for acquiring bulk-rock and mineral data. We are grateful to the constructive comments of Dr. Michael Roden and an anonymous reviewer. This work was supported by the National Natural Science Foundation of China (NSFC Grants 41130314, 91014003, 41630968, 41776067), Chinese Academy of Sciences (Innovation Grant Y42217101L), grants from Qingdao National Laboratory for Marine Science and Technology (2015ASKJ03) and NSFC-Shandong Joint Fund for Marine Science Research Centers (U1606401).

References

Blundy, J.D., Robinson, J.A.C., Wood, B.J., 1998. Heavy REE are compatible in clinopyroxene on the spinel lherzolite solidus. Earth and Planetary Science Letters 160, 493-504.

Blundy, J.D., Cashman, K., 2001. Ascent-driven crystallization of dacite magmas at Mount St Helens, 1980-1986. Contributions to Mineralogy and Petrology 140, 631-650.

Blundy, J.D., Cashman, K., 2005. Rapid decompression-driven crystallization recorded by melt inclusions from Mount St Helens volcano. Geology 33, 793-796.

Cashman, K., Blundy, J.D., 2000. Degassing and crystallization of ascending andesite and dacite. Philosophical Transactions of the Royal Society of London 358, 1487-1513.

Chen, X.M., Chen, L.H., Xu, X.S., 2009. Study on the genesis of clinopyroxene megacrysts in the Cenozoic alkali basalt at Changle，Shandong Province．Acta Petrologica Sinica，25(5)：1105-1116. (in Chinese with English abstract)

Chung, S.-L., Sun, S.-s., Tu, K., Chen, C.-H., Lee, C.-y., 1994. Late Cenozoic basaltic volcanism around the Taiwan Strait, SE China: product of lithosphere-asthenosphere interaction during continental extension. Chemical Geology 112, 1-20.

Demouchy, S., Jacobsen, S.D., Gaillard, F., Stern, C.R., 2006. Rapid magma ascent recorded by water diffusion profiles in mantle olivine. Geology 34, 429-432.

Dobosi, G., 1989. Clinopyroxene zoning patterns in the young alkali basalts of Hungary and their petrogenetic significance. Contributions to Mineralogy and Petrology 101, 112-121.

Geiger, H., Barker, A. K., Troll, V. R., 2016. Locating the depth of magma supply for volcanic eruptions, insights from Mt. Cameroon. Scientific reports 6, 33629.

Green, D.H., Ringwood, A.E., 1967. The genesis of basaltic magmas. Contributions to Mineralogy and Petrology 15, 103-190.

Gonnermann, H.M., Manga, M., 2013. Dynamics of magma ascent in the volcanic conduit, in: Fagents, S.A., Gregg, T.K.P., Lopes, R.M.C. (Eds.), Modeling volcanic processes: The physics and mathematics of volcanism. Cambridge University Press,

pp. 55-84.

Guo, P., Niu, Y., Sun, P., Ye, L., Liu, J., Zhang, Y., Feng, Y.-X., Zhao, J.-X., 2016. The origin of Cenozoic basalts from central Inner Mongolia, East China: The consequence of recent mantle metasomatism genetically associated with seismically observed paleo-Pacific slab in the mantle transition zone. Lithos 240-243, 104-118.

Herzberg, C., 1993. Lithosphere peridotites of the Kaapvaalcraton. Earth and Planetary Science Letters 120, 13-29.

Higgins, M.D., Allen, J.M., 1985. A new locality for primary xenolith-bearing nephelinites in northwestern British Columbia. Canadian Journal of Earth Sciences 22, 1556-1559.

Ho, K.S., Chen, J.C., Lo, C.H., Zhao, H.L., 2003. ^{40}Ar-^{39}Ar dating and geochemical characteristics of late Cenozoic basaltic rocks from the Zhejiang-Fujian region, SE China: eruption ages, magma evolution and petrogenesis. Chemical Geology 197, 287-318.

Huang, X.-L., Xu, Y.-G., Lo, C.-H., Wang, R.-C., Lin, C.-Y., 2007. Exsolution lamellae in a clinopyroxene megacryst aggregate from Cenozoic basalt, Leizhou Peninsula, South China: petrography and chemical evolution. Contributions to Mineralogy and Petrology 154, 691-705.

Huang, X., Niu, Y., Xu, Y., Ma, J., Qiu, H., Zhong, J., 2013. Geochronology and geochemistry of Cenozoic basalts from eastern Guangdong, SE China: constraints on the lithosphere evolution beneath the northern margin of the South China Sea.

Contributions to Mineralogy and Petrology 165, 437-455.

Irving, A.J., 1978. Flow crystallization: A mechanism for fractionation of primary magmas at mantle pressures [abs.]. American Geophysical Union Transactions 59, 1214.

Irving, A.J., 1980. Petrology and geochemistry of composite ultramafic xenoliths in alkali basalts and implications for magmatic processes within the mantle. American Journal of Science 280, 389-426.

Irving, A.J., Price, R.C. (1981) Geochemistry and evolution of Iherzolite-bearing phonolitic lavas from Nigeria, Australia, East Germany and New Zealand. *Geochimica et Cosmochimica Acta* **45**, 1309-1320.

Irving, A.J., Frey, F.A., 1984. Trace element abundances in megacrysts and their host basalts: Constraints on partition coefficients and megacryst genesis. Geochimica et Cosmochimica Acta 48, 1201-1221.

Lensky, N.G., Niebo, R.W., Holloway, J.R., Lyakhovsky, V., Navon, O., 2006. Bubble nucleation as a trigger for xenolith entrapment in mantle melts. Earth and Planetary Science Letters 245, 278-288.

Li, S., Mooney, W.D., Fan, Q., 2006. Crustal structure of mainland China from deep seismic sounding data. Tectonophysics 420, 239-252.

Liu, Y., Hu, Z., Gao, S., Günther, D., Xu, J., Gao, C., Chen, H., 2008. In situ analysis of major and trace elements of anhydrous minerals by LA-ICP-MS without applying an internal standard. Chemical Geology 257, 34-43.

McBride, J.S., Lambert, D.D., Nicholls, I.A., Price, R.C., 2001. Osmium Isotopic

Evidence for Crust–Mantle Interaction in the Genesis of Continental Intraplate Basalts from the Newer Volcanics Province, Southeastern Australia. Journal of Petrology 42, 1197-1218.

Mather, K.A., Pearson, D.G, Mckenzie, D., Kjarsgaard, B.A., Priestley, K., 2011. Constraints on the depth and thermal history of cratonic lithosphere from peridotite xenoliths, xenocrysts and seismology. Lithos 125, 729-742.

Meng, F., Gao, S., Niu, Y., Liu, Y., Wang, X., 2015. Mesozoic–Cenozoic mantle evolution beneath the North China Craton: A new perspective from Hf–Nd isotopes of basalts. Gondwana Research 27, 1574-1585.

Menzies, M.A., 1983. Mantle ultramafic xenoliths in alkaline magmas: Evidence for mantle heterogeneity modified by magmatic activity, in: Hawkesworth, C.J., Norry, M.J. (Eds.), Continental Basalts and Mantle xenoliths. Shiva Publishing, UK, pp. 92-110.

Menzies, M.A., Xu, Y., Zhang, H., Fan, W., 2007. Integration of geology, geophysics and geochemistry: A key to understanding the North China Craton. Lithos 96, 1-21.

Nakagawa, M., Wada, K., Wood, C. P., 2002. Mixed Magmas, Mush Chambers and Eruption Triggers: Evidence from Zoned Clinopyroxene Phenocrysts in Andesitic Scoria from the 1995 Eruptions of Ruapehu Volcano, New Zealand. Journal of Petrology 43, 2279-2303.

Neumann, E.R., Wulff-Pedersen, E., Simonsen, S.L., Pearson, N.J., Martí, J., Mitjavila, J., 1999. Evidence for Fractional Crystallization of Periodically Refilled Magma Chambers in Tenerife, Canary Islands. Journal of Petrology 40, 1089-1123.

Nickel, K.G., Brey, G., 1984. Subsolidus orthopyroxene-clinopyroxene systematics in the system CaO-MgO-SiO_2 to 60 kb: a reevaluation of the regular solution model. Contributions to Mineralogy and Petrology 87, 35-42.

Nimis, P., 1995. A clinopyroxene geobarometer for basaltic systems based on crystal-structure modeling. Contributions to Mineralogy and Petrology 121, 115-125.

Nimis, P., 1999. Clinopyroxene geobarometry of magmatic rocks. Part 2. Structural geobarometers for basic to acid, tholeiitic and mildly alkaline magmatic systems. Contributions to Mineralogy and Petrology 135, 62-74.

Nimis, P., Taylor, W.R., 2000. Single clinopyroxene thermobarometry for garnet peridotites. Part I. Calibration and testing of a Cr-in-Cpx barometer and an enstatite-in-Cpx thermometer. Contributions to Mineralogy and Petrology 139, 541-554.

Niu, Y., 1997. Mantle melting and melt extraction processes beneath ocean ridges: Evidence from abyssal peridotites. Journal of Petrology 38, 1047-1074.

Niu, Y., 2005. Generation and evolution of basaltic magmas: Some basic concepts and a hypothesis for the origin of the Mesozoic-Cenozoic volcanism in eastern China. Geological Journal of China Universities 11, 9-46.

Niu, Y., 2014. Geological understanding of plate tectonics: basic concepts, illustrations, examples and new perspectives. Global tectonics and metallogeny. 10, 23-46.

Niu, Y., 2016. The meaning of global ocean ridge basalt major element

compositions. Journal of Petrology 57, 2081-2104.

Niu, Y., Batiza, R., 1997. Trace element evidence from seamounts for recycled oceanic crust in the Eastern Pacific mantle. Earth and Planetary Science Letters 148, 471-483.

Niu, Y., O'Hara, M.J., 2003. Origin of ocean island basalts: A new perspective from petrology, geochemistry, and mineral physics considerations. Journal of Geophysical Research 108, 2209.

Niu, Y., O'Hara, M.J., 2007. Varying Ni in OIB olivines-product of process not source. Geochimica et Cosmochimica Acta 71, A721-A721.

Niu, Y., O'Hara, M.J., 2008. Global correlations of ocean ridge basalt chemistry with axial depth: A new perspective. Journal of Petrology 49, 633-664.

Niu, Y., O'Hara, M.J., 2009. MORB mantle hosts the missing Eu (Sr, Nb, Ta and Ti) in the continental crust: New perspectives on crustal growth, crust-mantle differentiation and chemical structure of oceanic upper mantle. Lithos 112, 1-17.

Niu, Y., Gilmore, T., Mackie, S., Greig, A., Bach, W., 2002. Mineral chemistry, whole-rock compositions, and petrogenesis of Leg 176 gabbros: data and discussion. Proceedings of the Ocean Drilling Program, Scientific Results, 1-60.

Niu, Y., Wilson, M., Humphreys, E.R., O'Hara, M.J., 2011. The Origin of intra-plate ocean island basalts (OIB): The lid effect and its geodynamic implications. Journal of Petrology 52, 1443-1468.

Niu, Y., Wilson, M., Humphreys, E.R., O'Hara, M.J., 2012. A trace element perspective on the source of ocean island basalts (OIB) and fate of subducted ocean

crust (SOC) and mantle lithosphere (SML). Episodes 35, 310-327.

O'Hara, M.J., 1967. Mineral faces in ultrabasic rocks, in: Wyllie, P.J. (Ed.), Ultramafic and related rocks. John Wylie and Sons, New York, pp. 7-18.

O'Hara, M.J., 1977. Geochemical evolution during fractional crystallization of a periodically refilled magma chamber. Nature 266, 503-507.

O'Hara, M.J., Schairer, J.F., 1963. The join diopside-pyrope at atmospheric pressure. Carnegie Institution of Washington Yearbook 62, 107-115.

O'Hara, M.J., Mathews, R.E., 1981. Geochemical evolution in an advancing, periodically replenished, periodically tapped, continuously fractionated magma chamber. Journal of the Geological Society, London 138, 237-277.

O'Hara, M.J., Herzberg, C.T., 2002. Interpretations of trace element and isotope features of basalts: Relevance of field relations, major element data, phase equilibria and magma chamber modeling in basalt petrogenesis. Geochimica et Cosmochimica Acta 66, 2167-2191.

O'Reilly, S. Y., Griffin, W. L., 1984. Sr isotopic heterogeneity in primitive basaltic rocks, southeastern Australia: correlation with mantle metasomatism. Contributions to Mineralogy and Petrology 87, 220-230.

O'Reilly, S.Y., Griffin, W.L., 2010. Rates of Magma Ascent: Constraints from Mantle-Derived Xenoliths, in: Dosseto, A., Turner, S.P., Van Orman, J.A. (Eds.), Timescales of Magmatic Processes: From Core to Atmosphere. John Wylie and Sons, Ltd, Chichester, UK., pp. 116-123.

Putirka, K.D., Johnson, M.C., Kinzler, R.J., Longhi, J., Walker, D., 1996.

Thermobarometry of mafic igneous rocks based on clinopyroxene-liquid equilibria, 0-30 kb. Contributions to Mineralogy and Petrology 123, 92-108.

Putirka K.D., Mikaelian, H., Ryerson, F., Shaw, H., 2003. New clinopyroxene-liquid thermobarometers for mafic, evolved, and volatile-bearing lava compositions, with applications to lavas from Tibet and the Snake River Plain, Idaho. American Mineralogist, 1542.

Putirka, K.D., 2008. Thermometers and barometers for volcanic systems, in: Putirka, K.D., Tepley, F. (Eds.), Minerals, Inclusions and Volcanic Processes. The Mineralogist Society of America 69, pp. 61-120.

Rudnick, L.R., McDonough, W.F., O'Connel, R.J., 1998. Thermal structure, thickness and composition of continental lithosphere. Chemical Geology 145, 395-411.

Sigmarsson, O., Carn, S., Carracedo, J.C., 1998. Systematics of U-series nuclides in primitive lavas from the 1730–36 eruption on Lanzarote, Canary Islands, and implications for the role of garnet pyroxenites during oceanic basalt formations. Earth and Planetary Science Letters 162, 137-151.

Sleep, N.H., 2005. Evolution of continental lithosphere. Annual Review of Earth and Planetary Sciences 33, 369-393.

Sobolev, A.V., Hofmann, A.W., Sobolev, S.V., Nikogosian, I.K., 2005. An olivine-free mantle source of Hawaii shield basalts. Nature 434, 590-597.

Sobolev, A.V., Hofmann, A.W., Kuzmin, D.V. et al., 2007. The amount of recycled crust in sources of mantle-derived melts. Science 316, 412-417.

Song, S., Su, L., Li, X., Zhang, G., Niu, Y., Zhang, L., 2010. Tracing the 850-Ma continental flood basalts from a piece of subducted continental crust in the North

Qaidam UHPM belt, NW China. Precambrian Research 183, 805-816.

Sparks, R.S.J., Huppert, H.E., Turner, J.S., Sakuyama, M., O'Hara, M.J., 1984. The fluid dynamics of evolving magma chambers [and discussion]. Philosophical Transactions of the Royal Society of London 310, 511-534.

Sparks, R.S.J., Murphy, M.D., Lejeune, A.M., Watts, R.B., Barclay, J., Young, S.R., 2000. Control on the emplacement of the andesite lava dome of the Soufrière Hills volcano, Montserrat by degassing-induced crystallization. Terra Nova 12, 14-20.

Spera, F.J., 1984. Carbon dioxide in petrogenesis III: Role of volatiles in the ascent of alkaline magma with special reference to xenolith-bearing mafic lavas. Contributions to Mineralogy and Petrology 88, 217-232.

Stock, M. J., Taylor, R. N., Gernon, T. M., 2012. Triggering of major eruptions recorded by actively forming cumulates. Scientific reports 2, 731.

Sun, P., Niu, Y., Guo, P., Ye, L., Liu, J. Feng, Y. , 2017. Elemental and Sr–Nd–Pb isotope geochemistry of the Cenozoic basalts in Southeast China: Insights into their mantle sources and melting processes. Lithos 272–273, 16-30.

Sun, S.S., McDonough, W.F., 1989. Chemical and isotopic systematic of oceanic basalts: Implications for mantle composition and processes, in: Saudersand, A.D., Norry, M.J. (Eds.), Magmatism in Ocean Basins. London: Geological Society London Special Publications, 313-345.

Tu, K., Flower, M. F., Carlson, R. W., Zhang, M., Xie, G., 1991. Sr, Nd, and Pb isotopic compositions of Hainan basalts (south China): implications for a subcontinental lithosphere Dupal source. Geology 19, 567-569.

Wang, X., Li, Z., Li, X., Li, J., Liu, Y., Long, W., Zhou, J., Wang, F., 2011.

Temperature, pressure, and composition of the mantle source region of Late Cenozoic basalts in Hainan Island, SE Asia: A consequence of a young thermal mantle plume close to subduction zones? Journal of Petrology 53, 177-233.

Wass, S.Y., 1979. Mutiple origins of clinopyroxenes in alkali basaltic rocks. Lithos 12, 115-132.

Wass, S.Y., 1980. Geochemistry and origin of xenolith-bearing and related alkali basaltic rocks from the southern Highlands, New South Wales, Australia. American Journal of Science 280, 639 - 666.

Wood, B.J., Banno, S., 1973. Garnet-orthopyroxene and orthopyroxene relationships in simple and complex systems. Contributions to Mineralogy and Petrology 42, 109-124.

Woods, A.W., Cardoso, S.S.S., 1997. Triggering basaltic volcanic eruptions by bubble-melt separation. Nature 385, 518-520.

Xiao, Y., Niu, Y., Chen, S., Wang, X., Xue, Q., Wang, G., Gao, Y., Gong, H., Kong, J., Guo, P., Shao, F., Sun, P., Duan, M., Hong, D., Wang, D., 2018. Mineral chemistry constraints on the petrogenesis of syn-collisional granitoids with mafic magmatic enclaves and their implications. (in preparation)

Yang, Z.F., Zhou, J.H., 2013. Can we identify source lithology of basalt? Scientific Reports 3, 1-7.

Zhang, Z., Wang, Y., 2007. Crustal structure and contact relationship revealed from deep seismic sounding data in South China. Physics of the earth and planetary interiors 165, 114-126.

Zheng, J., O'Reilly, S. Y., Griffin, W. L., Lu, F., Zhang, M., Pearson, N. J., 2001. Relict refractory mantle beneath the eastern North China block: significance for lithosphere evolution. Lithos 57, 43-66.

Zou, H., Zindler, A., Xu, X., Qi, Q., 2000. Major, trace element, and Nd, Sr and Pb isotope studies of Cenozoic basalts in SE China: mantle sources, regional variations, and tectonic significance. Chemical Geology 171, 33-47.

Figure captions:

Fig. 1. (a) Distribution of the Cenozoic volcanism in eastern China. (b) Locations of our samples from Southeast (SE) China. Modified from Sun et al. (2017).

Fig. 2. Hand specimens of mantle xenoliths (a & b) and clinopyroxene megacrysts (c & d) hosted in basalts from SE China. Photomicrographs of the clinopyroxene megacrysts (e & f) and abundant olivine phenocrysts of varying size (g & h) in these basalts.

Fig. 3. TAS diagram showing compositional variations of the SE China basalts of this study.

Fig. 4. $Mg^{\#}$ variation diagrams of Na_2O+K_2O, TiO_2, P_2O_5, CaO/Al_2O_3, Cr, Ni, La, Sm, La/Sm and Sm/Yb of basalt samples from Jiucaidi as an example (more samples with larger compositional variation available than other locations), which is consistent with varying extent of Ol-Cpx crystallization.

Fig. 5. Chondrite-normalized REE patterns (a) and primitive mantle-normalized multiple incompatible element abundances (b). For comparison, average composition of present-day OIB (Sun and McDonough, 1989) are plotted. These basalts are

extremely enriched in incompatible elements, indicative of their enriched source character.

Fig. 6. (a) Compositions of all analyzed clinopyroxene data points (n = 231). These clinopyroxenes vary compositionally in the range of Wo_{35-47}, En_{35-53}, Fs_{9-19}. (b) Chemical profile of clinopyroxene megacryst interior (sample PY-XD-07I as an example) to show homogeneous compositions in a given clinopyroxene crystal.

Fig. 7. Co-variations of $Mg^{\#}$ with major elements (SiO_2, TiO_2, Al_2O_3, FeO, Na_2O) and Cr of the clinopyroxene megacrysts. These clinopyroxene megacrysts were crystallized from melts that had experienced variable extent of fractional crystallization. Three clinopyroxene megacrysts from Jiucaidi and Xiadai (JC11-03A, XD11-11A and XD11-11C) have apparent lower $Mg^{\#}$ (65 – 69), SiO_2 and Cr, and higher TiO_2, Al_2O_3, FeO and Na_2O, compared with other Cpx megacrysts ($Mg^{\#}$ = 75 – 84), reflecting their crystallization from compositionally more evolved melts.

Fig. 8. (a) Equilibrium tests between Cpx megacrysts from Jiucaidi as an example and host bulk-rock uncorrected for the olivine effect with $Mg^{\#}$ of 56, 60 and 65. (b) Equilibrium tests between Cpx megacrysts from Jiucaidi and host bulk-rock corrected for the olivine effect with $Mg^{\#}$ of 48, 53 and 59. Both tests (a, b) use a $K_D[Fe\text{-}Mg]^{Cpx\text{-}melt}$ = 0.28 ± 0.08 to define the equilibrium envelope (Putirka, 2008) and only data points falling within the equilibrium envelope are used for further thermobarometry calculations. (c) Calculated Cpx temperatures and pressures using uncorrected bulk-rock compositions. (d) Calculated Cpx temperatures and pressures using bulk-rock compositions corrected for the olivine effect. The Cpx thermometer and barometer we use are from Putirka et al. (2003), with systematic errors of ~ ± 33 ℃ and ± 1.7 kbar, respectively.

Fig. 9. Calculated equilibrium temperatures and pressures of clinopyroxene

megacrysts in *P-T* space. The Cpx barometer and thermometer we use are recalibrated from Nimis (1995) and Nimis and Taylor (2000), with systematic errors of ~ ± 3.1 kbar and ± 58 ℃, respectively (Putirka, 2008; equation 32a/32d). Standard errors of *P* and *T* results calculated from multiple analyses in a single Cpx are also plotted, respectively. For comparison, the lithosphere geotherm of eastern China (Menzies et al., 2007) and the solidus and liquidus of alkali olivine basalt (Green and Ringwood, 1967) are also plotted. The significantly higher temperatures of xenolith-bearing melts relative to the ambient mantle lithosphere ensure cooling-induced crystallization to be an unavoidable consequence during ascent.

Fig. 10. Cartoon showing the evolution and ascent paths of mantle xenolith-bearing magmas prior to their eruption. Incompatible element- and volatile- (H_2O and CO_2) enriched melts are generated from low extent melting of a fertile mantle source. These melts are then extracted and gathered in the magma chambers under the conditions of lithospheric mantle, where variable extent of crystallization of olivine and clinopyroxene happens. After extraction from the magma chambers, these melts will exsolve volatiles, resulting in bulk magma volume expansion, and development of power to fragment the conduit wall-rock to produce “mantle xenoliths”, and rapidly transport them to the surface with limited residence in shallow levels.

Highlights

1. Xenolith-bearing alkali basalts experienced crystallization during rapid ascent.
2. Such crystallization is largely cooling-induced.
3. The crystallization happened in the magma chambers within the lithospheric mantle.
4. The host melt experienced limited low-pressure residence in the shallow levels.

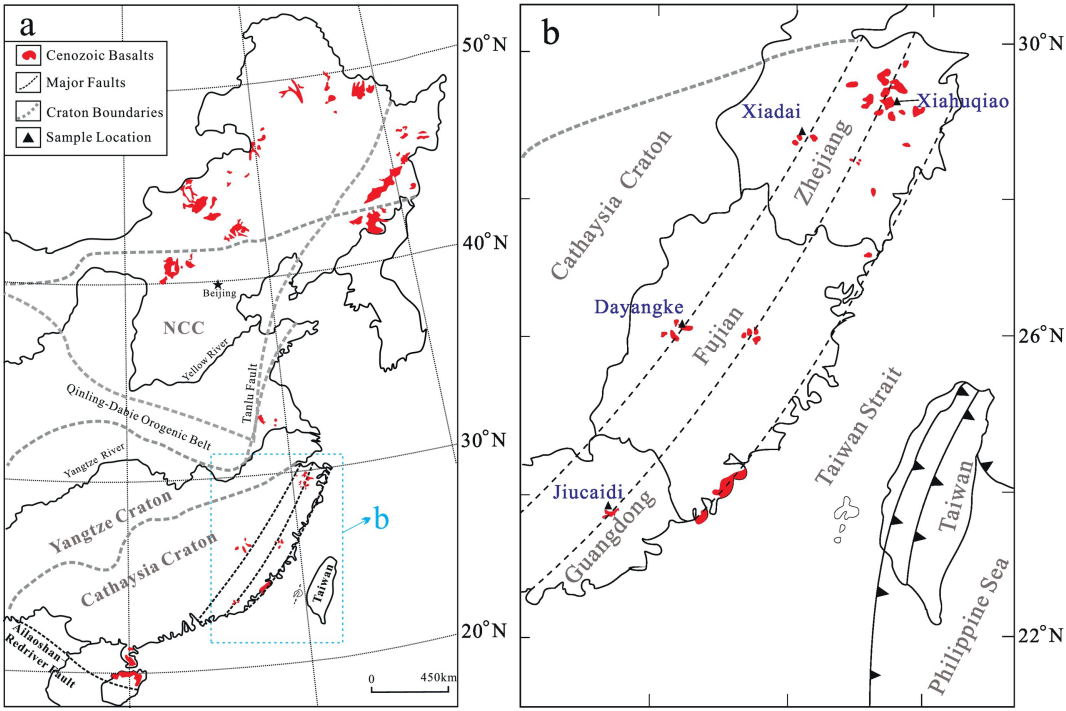
a
Cenozoic Basalts
Major Faults
Craton Boundaries
Sample Location
110°E
120°E
130°E
50°N
40°N
30°N
20°N
Beijing
NCC
Yellow River
Tanlu Fault
Qinling-Dabie Orogenic Belt
Yangtze River
Yangtze Craton
Cathaysia Craton
Taiwan
Ailaoshan
Redriver Fault
0
450km
b
117°E
119°E
121°E
30°N
26°N
22°N
Xiadai
Xiahuqiao
Cathaysia Craton
Zhejiang
Dayangke
Fujian
Taiwan Strait
Jiucaidi
Guangdong
Taiwan
Philippine Sea

Figure 1

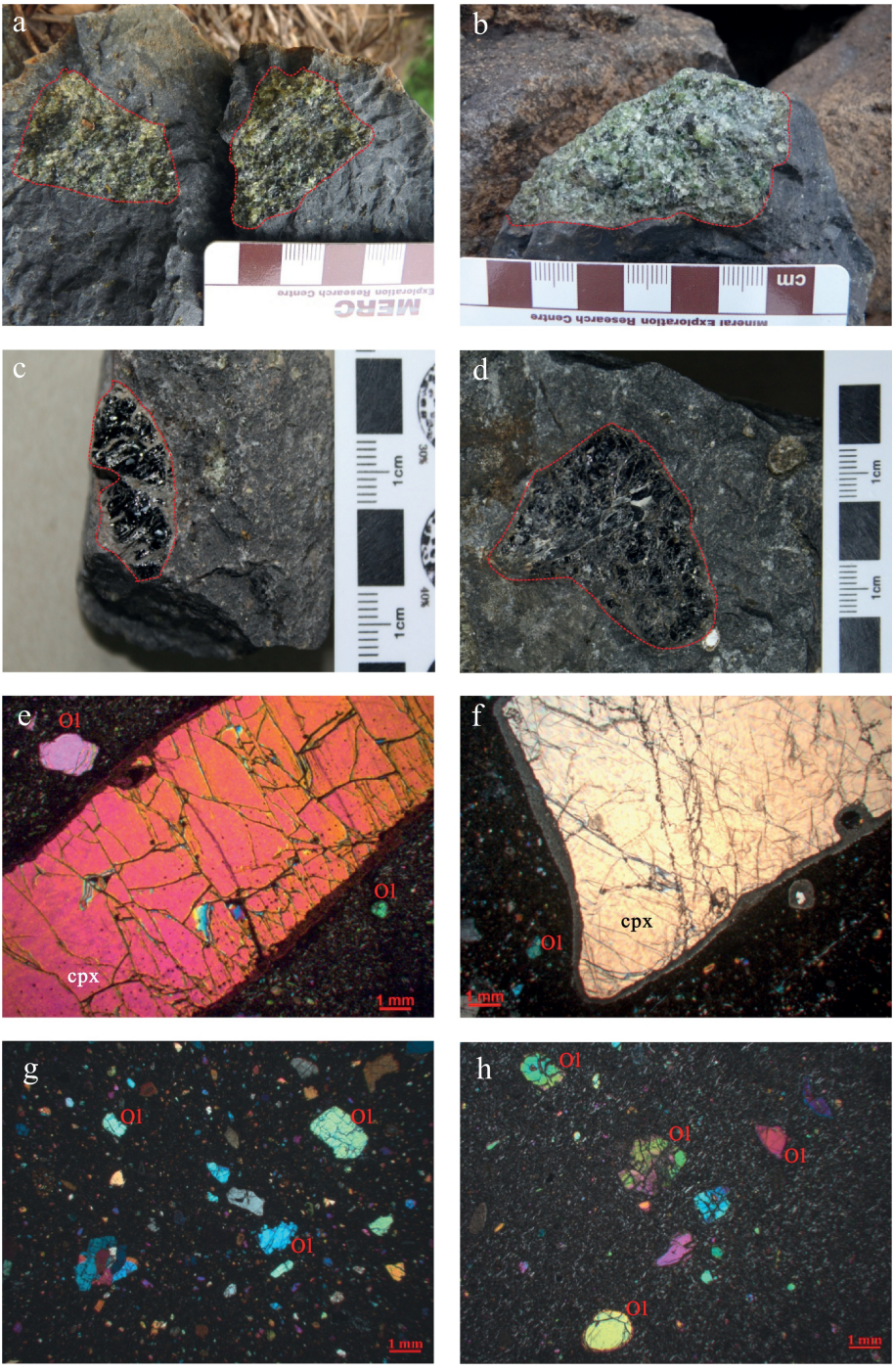

Figure 2

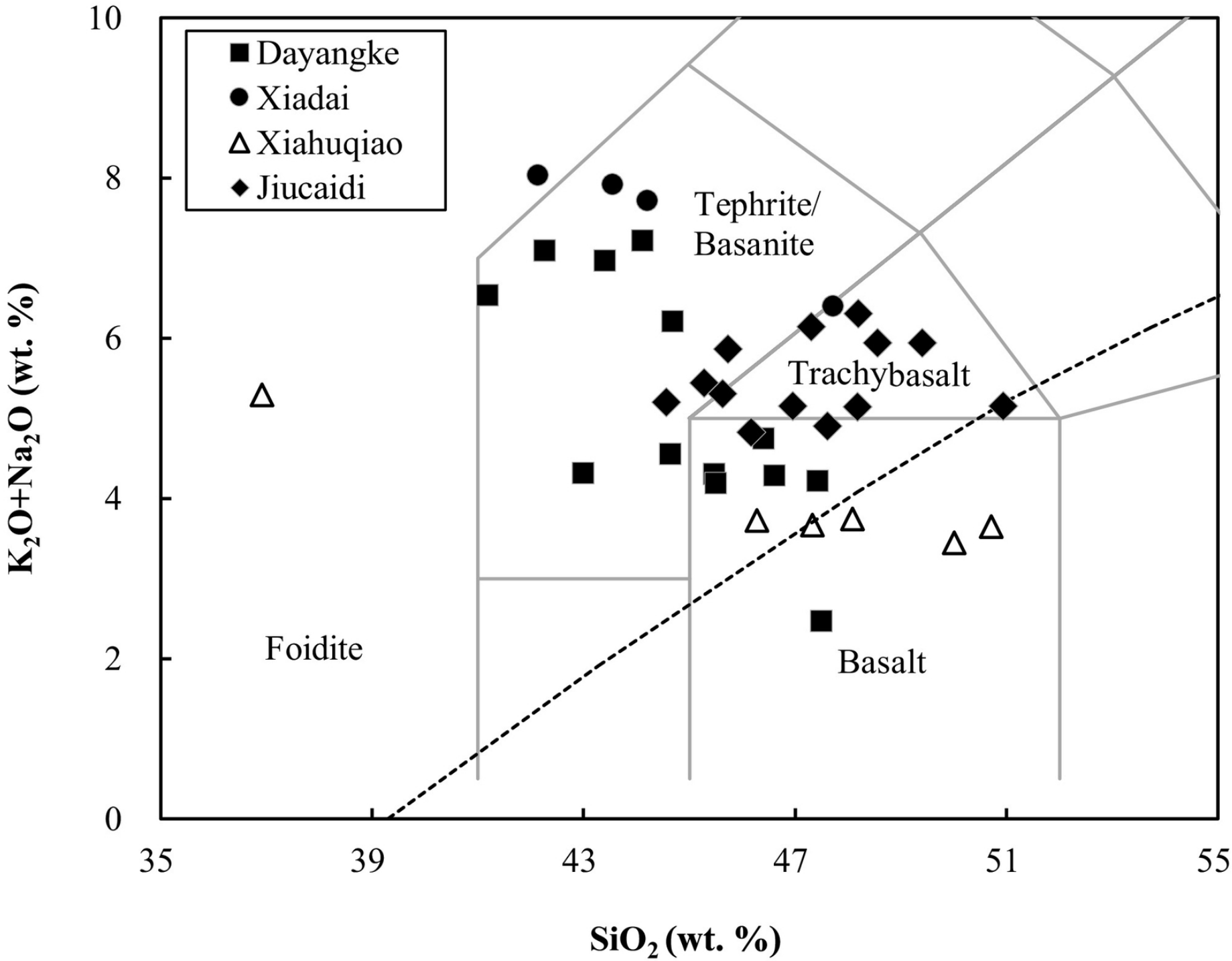
Dayangke
Xiadai
Xiahuqiao
Jiucaidi
Tephrite/
Basanite
Trachybasalt
Foidite
Basalt
10
8
6
4
2
0
35
39
43
47
51
55
K2O+Na2O (wt. %)
SiO2 (wt. %)

Figure 3

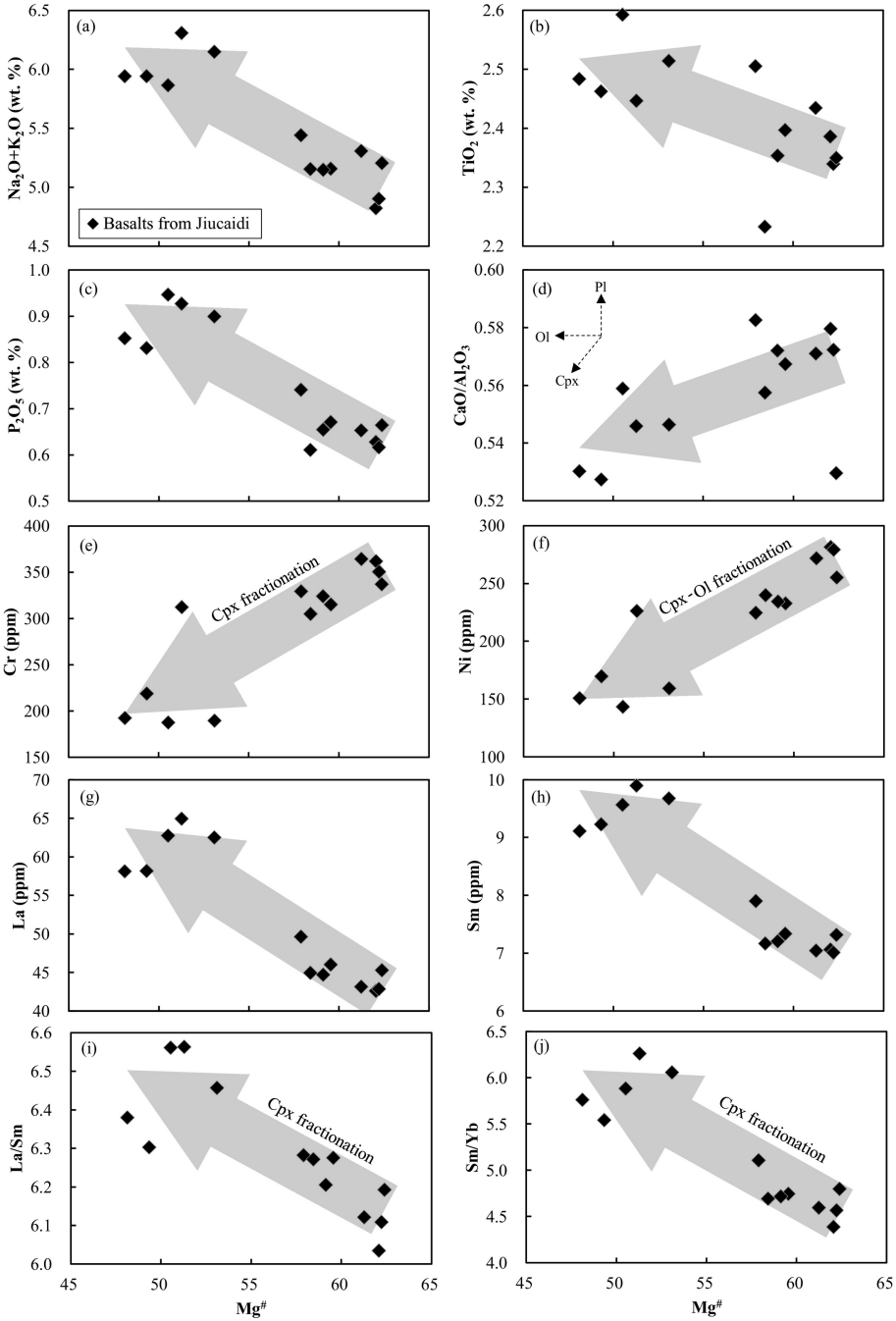
(a)
Basalts from Jiucaidi
Na_2O+K_2O (wt. %)
(b)
TiO_2 (wt. %)
(c)
P_2O_5 (wt. %)
(d)
Pl
Ol
Cpx
CaO/Al_2O_3
(e)
Cpx fractionation
Cr (ppm)
(f)
Cpx-Ol fractionation
Ni (ppm)
(g)
La (ppm)
(h)
Sm (ppm)
(i)
Cpx fractionation
La/Sm
(j)
Cpx fractionation
Sm/Yb
Mg#
Mg#

Figure 4

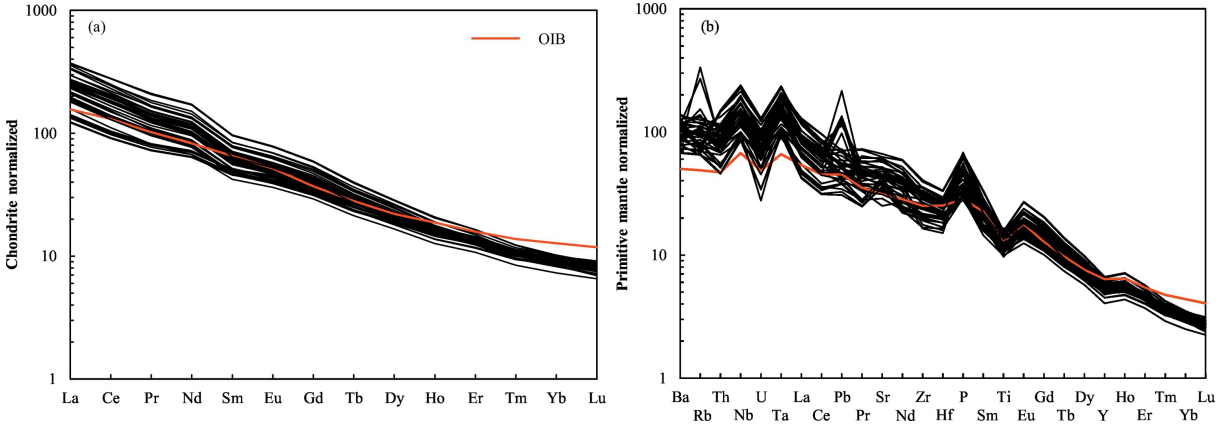
(a)
OIB
Chondrite normalized
1000
100
10
1
La Ce Pr Nd Sm Eu Gd Tb Dy Ho Er Tm Yb Lu
(b)
Primitive mantle normalized
1000
100
10
1
Ba Th U La Pb Sr Zr P Ti Gd Dy Ho Tm Lu
Rb Nb Ta Ce Pr Nd Hf Sm Eu Tb Y Er Yb

Figure 5

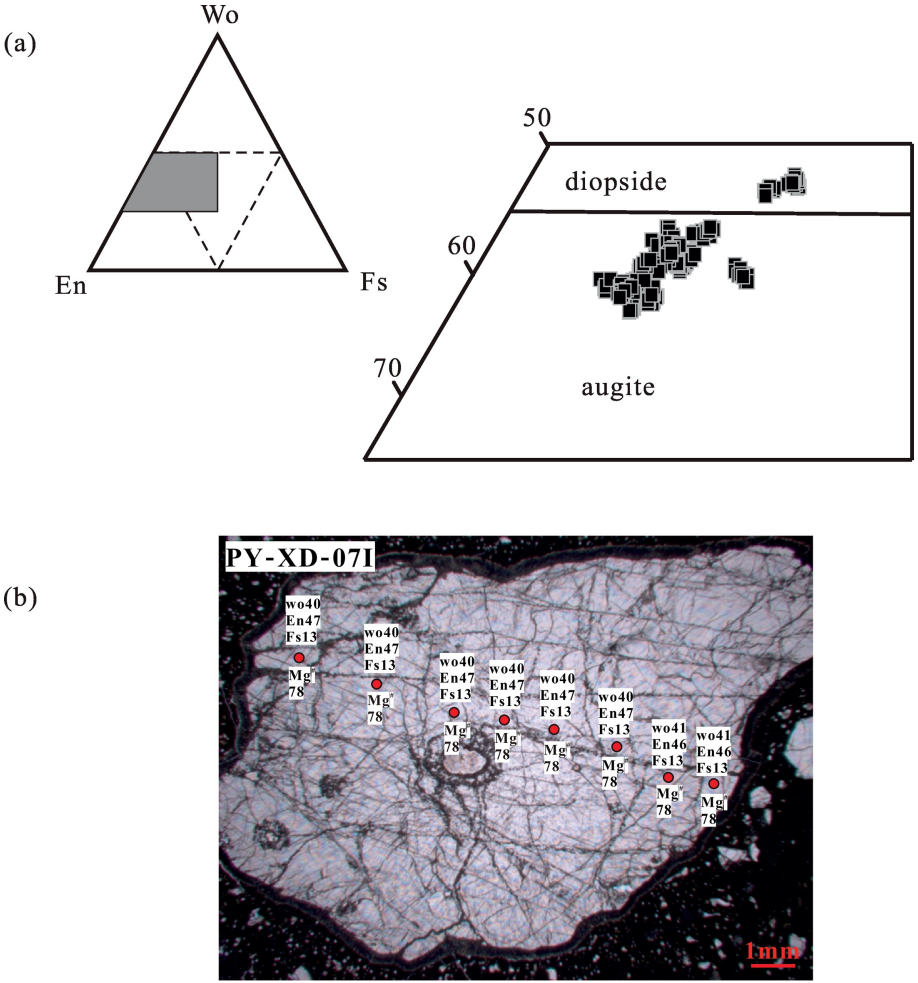
(a)
Wo
En
Fs
50
60
70
diopside
augite
(b)
PY-XD-07I
wo40 En47 Fs13 Mg# 78
wo41 En46 Fs13 Mg# 78
1mm

Figure 6

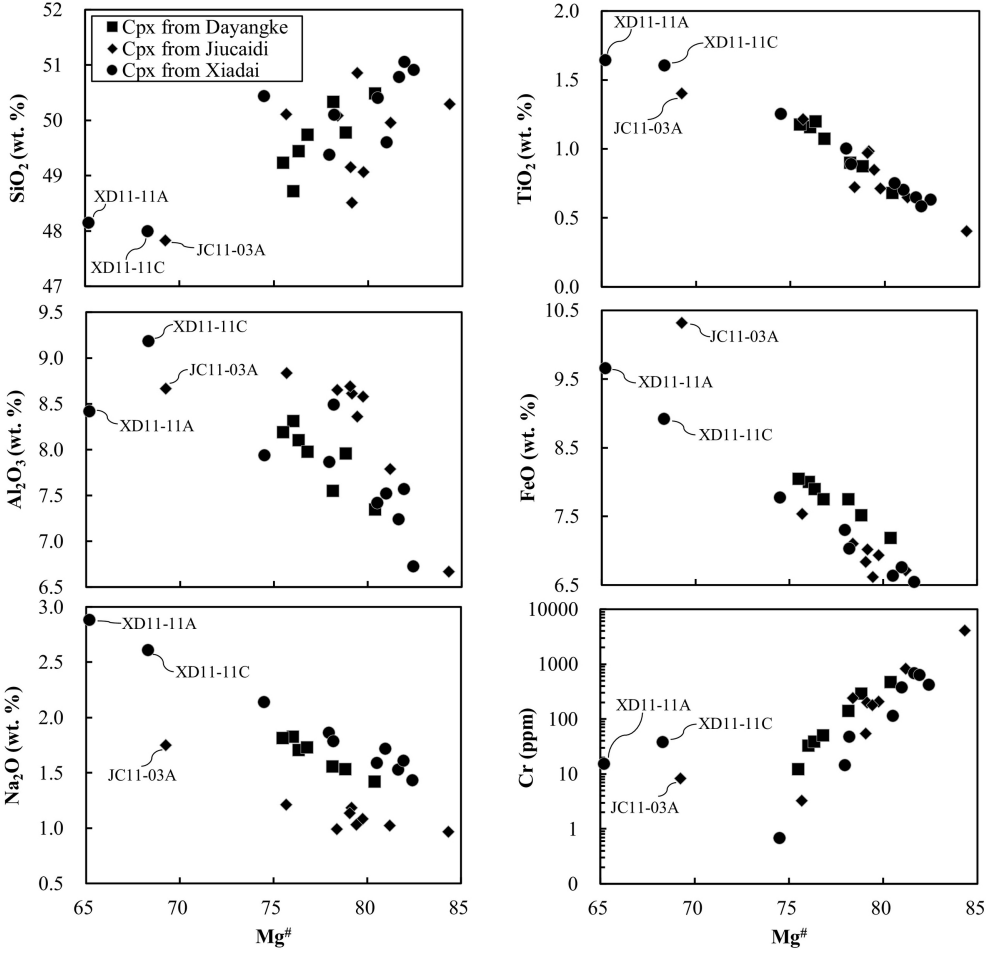
Cpx from Dayangke
Cpx from Jiucaidi
Cpx from Xiadai
SiO2 (wt. %)
TiO2 (wt. %)
Al2O3 (wt. %)
FeO (wt. %)
Na2O (wt. %)
Cr (ppm)
Mg#
XD11-11A
XD11-11C
JC11-03A

Figure 7

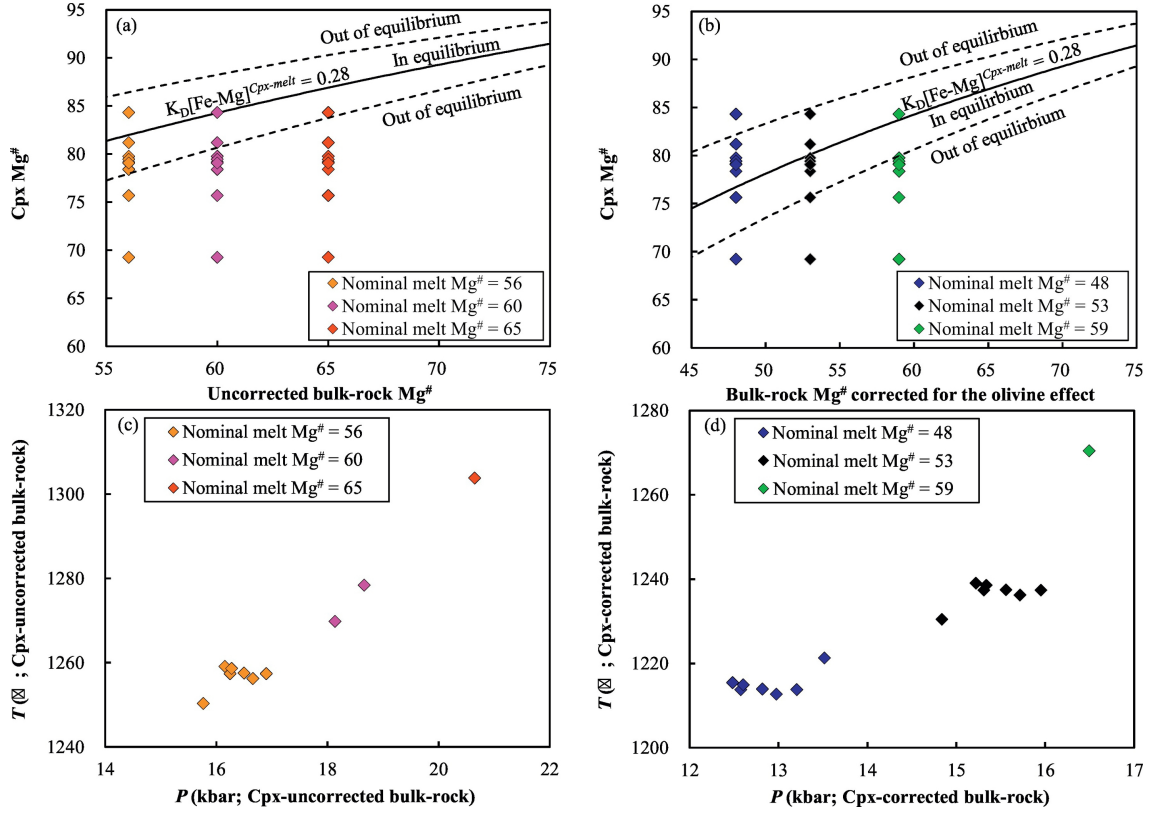
(a)
Out of equilibrium
In equilibrium
Out of equilibrium
$K_D[Fe\text{-}Mg]^{Cpx\text{-}melt} = 0.28$
Nominal melt Mg# = 56
Nominal melt Mg# = 60
Nominal melt Mg# = 65
Cpx Mg#
Uncorrected bulk-rock Mg#
(b)
Out of equilirbium
In equilirbium
Out of equilirbium
$K_D[Fe\text{-}Mg]^{Cpx\text{-}melt} = 0.28$
Nominal melt Mg# = 48
Nominal melt Mg# = 53
Nominal melt Mg# = 59
Cpx Mg#
Bulk-rock Mg# corrected for the olivine effect
(c)
Nominal melt Mg# = 56
Nominal melt Mg# = 60
Nominal melt Mg# = 65
T (☒ ; Cpx-uncorrected bulk-rock)
P (kbar; Cpx-uncorrected bulk-rock)
(d)
Nominal melt Mg# = 48
Nominal melt Mg# = 53
Nominal melt Mg# = 59
T (☒ ; Cpx-corrected bulk-rock)
P (kbar; Cpx-corrected bulk-rock)

Figure 8

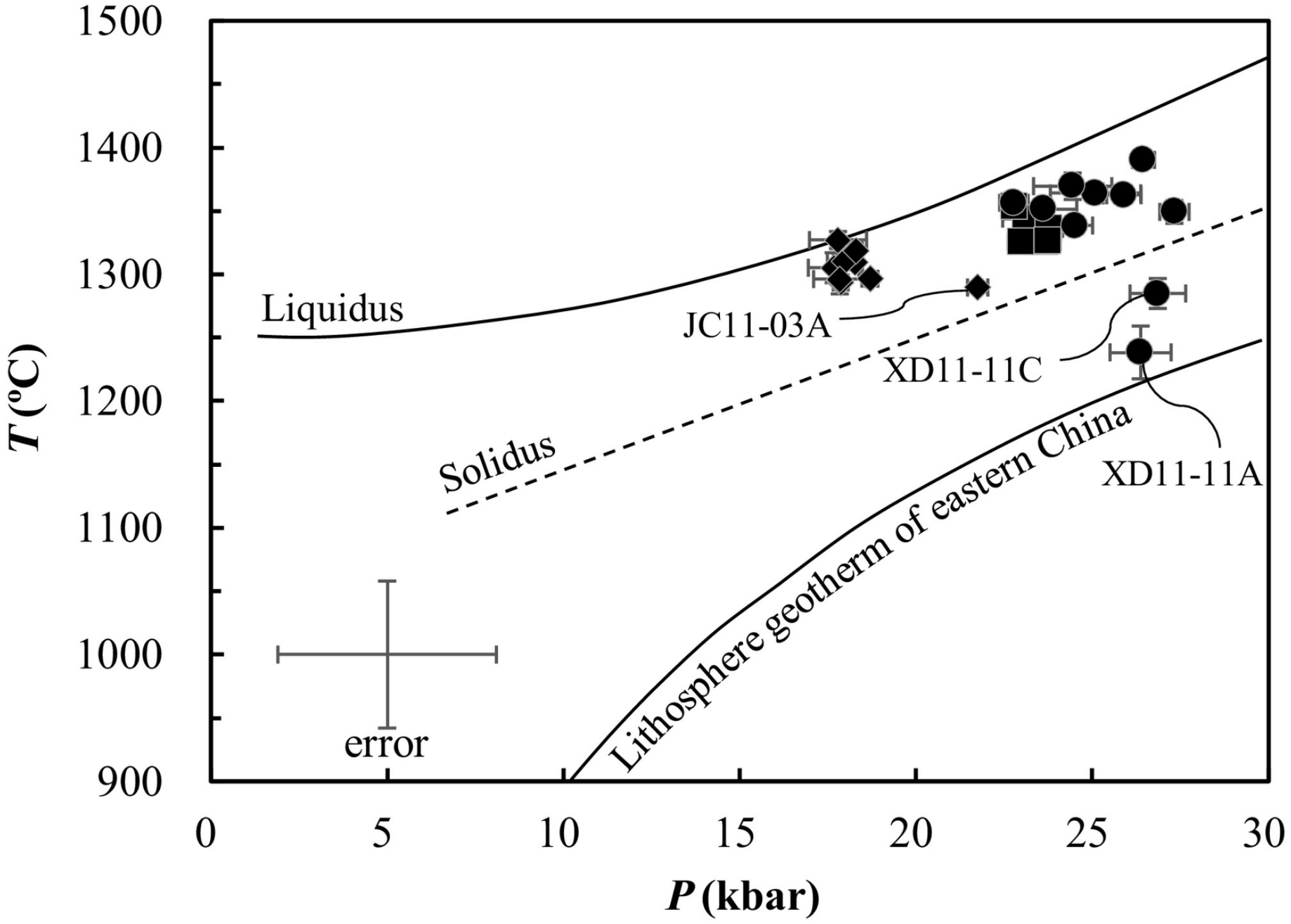
1500
1400
1300
1200
1100
1000
900
T (ºC)
0
5
10
15
20
25
30
P (kbar)
Liquidus
Solidus
JC11-03A
XD11-11C
XD11-11A
Lithosphere geotherm of eastern China
error

Figure 9

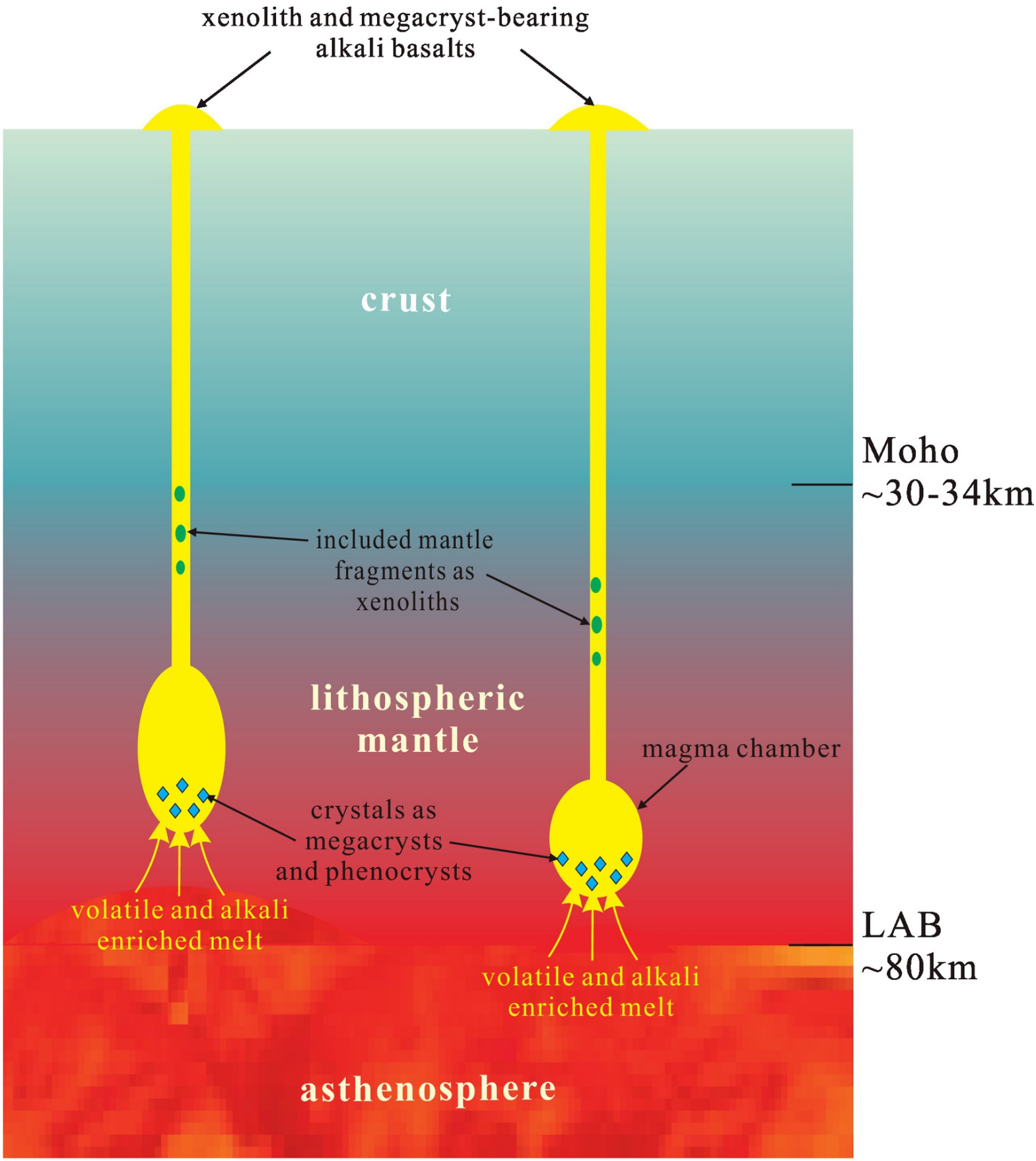
xenolith and megacryst-bearing
alkali basalts
crust
Moho
~30-34km
included mantle
fragments as
xenoliths
lithospheric
mantle
magma chamber
crystals as
megacrysts
and phenocrysts
volatile and alkali
enriched melt
LAB
~80km
volatile and alkali
enriched melt
asthenosphere

Figure 10